17èmes JOURNEES DE L'HYDRODYNAMIQUE
JH2020

24 - 26 novembre 2020
CHERBOURG - en - COTENTIN

Comparison of bathymetry variation effects on tidal turbine behaviour

Effet de variations bathymétriques sur le fonctionnement d'une hydrolienne

Maëlys Magnier[1,2], Philippe Druault[1], Benoît Gaurier[2], and Grégory Germain[2,*]

[(1)]Sorbonne Université, CNRS, UMR 7190, Institut Jean Le Rond d'Alembert, F-75005 Paris, France
[(2)]Ifremer, Marine Structure Laboratory, 150 Quai Gambetta 62200 Boulogne sur Mer, France
[*]Corresponding author: gregory.germain@ifremer.fr

Résumé

Les zones à forts courants de marée exploitables avec des hydroliennes présentent souvent des bathymétries complexes où l'intensité turbulente des courants peut atteindre des valeurs très élevées. Afin d'étudier les effets des variations de courants induites par les variations bathymétriques sur le fonctionnement d'une hydrolienne, un dispositif expérimental est développé dans le bassin à circulation de l'Ifremer. Le sillage de deux bathymétries, un cylindre à base carrée et un cube suivi de ce même cylindre, est caractérisé à partir de résultats de mesures PIV. Les résultats montrent que le sillage du cylindre est plus énergétique que celui de la configuration en tandem. Les structures tourbillonnaires qu'il émet remontent vers la surface contrairement à celles issues du tandem, le cube empêchant leur développement. Les effets de ces sillages sur une hydrolienne sont ensuite observés. A cette fin, une turbine est positionnée successivement à différentes positions dans le sillage des deux types d'obstacles étudiés précédemment. Les résultats obtenus montrent que les caractéristiques du sillage en terme d'organisation, d'échelle intégrale et de fréquence de détachement tourbillonnaire jouent un rôle majeur sur le fonctionnement d'une machine. Il est donc primordial de bien connaitre les caractéristiques des conditions de fonctionnement des hydroliennes pour garantir leur fonctionnement sur le long terme.

Summary

Areas with strong tidal currents that can be exploited with tidal turbines often have complex bathymetries where the turbulent intensity of these currents can reach very high values. To study the effects of bathymetric variations on the operation of a tidal turbine, an experimental device has been developed in the Ifremer circulation tank. The wake of two kinds of bathymetries, a cylinder with a square base and a cube followed by this same cylinder, are characterized and compared from PIV measurement results. The results show that the wake of the cylinder is more energetic than that of the tandem configuration. The vortex structures that it emits rise to the surface unlike those resulting from the tandem, the cube preventing their development. The effects of these wakes on a tidal turbine are then observed. To this aim, a turbine is positioned successively at different positions in the wake of obstacles placed at the bottom of the tank. The results obtained show that the characteristics of the wake in terms of organization, integral length scale and vortex detachment frequency play a major role in the operation of a machine. It is therefore essential to know the characteristics of the operating conditions of tidal turbines in order to guarantee their long-term operation.

1. Introduction

Each potential tidal area is unique and a lot of works has been carried out to characterize turbulent inflow specificities [1]. One of the main worst effect to tidal turbine is due to the presence of large scale energetic flow structures induced by bathymetry variations [2]. Indeed, the interaction of high velocity flows with bathymetry variations leads to the creation of flow structures which could notably impact the performance of a tidal turbine (structural load, blade fatigue...). Chamorro *et al.* [3] underlined the lack of study on the turbulent structures effect on turbines power production and wake meandering, especially for bathymetry generated structures. Blackmore *et al.* [4] and Mycek *et al.* [5] demonstrated that the increase of turbulence intensity and turbulence length scale slightly increase the power and thrust coefficients. In the wind energy sector, many papers have underlined the importance of studying the turbulent inflow impacting the wind turbines. Churchfield *et al.* [6] studied a wind turbine submitted to a stable and unstable flow with a high or low surface roughness. They concluded that vortex turbulent structures embedded in the flow cause loads fluctuations as significant as when the turbine is in the wake of another upstream turbine, justifying the interest of this kind of study for the specific case of tidal turbine.
Surface-mounted 2D elements (rib, horizontal cylinder or dune) are often used to represent simplified roughness elements in water [7]. The wake of such structures presents periodical Kelvin-Helmholtz vortices, generated from the upstream edge of the obstacle. These large scale periodic events, sometimes denoted kolk-vortices, can rise in the water column in the far wake of high aspect ratio obstacles [7, 8], contrary to cube wake (small wake with horizontal development). This underlines that large bathymetry (cylinder-like element) leads to generate large scale structures which potentially have negative effect on tidal turbine positioned in the wake [9]. In-situ, it is rare to encounter isolated regular obstacles even if bathymetry can show obstacles significantly higher than its neighbours. This work aims to study the effect of the accumulation of isolated obstacles on the global wake more precisely than the work done in [10], focus on aspect ratio influence of different kind of obstacles arrangement.

After presenting the experimental set-up, wakes generated behind two kinds of obstacles are compared. The effect of the addition of an upstream wall-mounted cube on the wake development of a cylinder is detailed in and out of the symmetry plane. Then, the effect of flow variations induced by the obstacles on a tidal turbine is analysed.

2. Experimental set up

2.1 Facility and test cases

Tests are carried out in the wave and current circulating flume tank of IFREMER located in Boulogne-sur-Mer (France). The test section is 18m long $\times$ 4m wide $\times$ 2m deep. The incoming flow (U_∞, V_∞, W_∞) is assumed to be steady and constant, with $U_\infty = 1\text{m.s}^{-1}$ and $V_\infty = W_\infty = 0$. The three instantaneous velocity components are denoted (U,V,W) along the (x,y,z) directions respectively (see figure 1). According to the Reynolds decomposition, each instantaneous velocity component is separated in a mean value and a fluctuating part: $U = \overline{U} + u^{'}$ where the overbar indicates the time average. A low turbulence intensity $I_\infty = 1.5\%$ is reached when a grid combined with a honeycomb is placed at the inlet of the working section [7] and the boundary layer height, calculated as follows $\delta = \delta_{95} = z\ (\overline{U} = 0.95 \times U_\infty)$, is equal to $\delta = 0.32m$.
During this study the wake of an isolatad square cylinder ($C6$) is compared to the one of a tandem configuration: a cube upstream a square cylinder ($C1$-$C6$) (see figure 2). Both the cylinder and the cube sections are a square of side H, with $H = 0.25m$. The cylinder is 6H long, corresponding to an aspect ratio of 6. The element spacing is fixed to $2H$ and the cube is located upstream of the cylinder. Such a spacing allows the shear layer separating from the cube to reattach on the downstream cylinder [11, 12]. The x-origin is set at the center of the cylinder. $z = 0$ corresponds to the wall. Obstacles are disposed symmetrically around the spanwise origin $y = 0$.
For the present investigation, the incoming flow Reynolds number is $Re = \frac{HU_\infty}{\nu} = 2.5 \times 10^5$ with ν the water

kinematic viscosity. The Froude number is $Fr = \frac{U_\infty}{\sqrt{g \times D_e}} = 0.23$ with D_e the flume tank depth and g the gravity. The scaled experiment has then non-dimensioned parameters similar to those of real sea conditions [7], for which the Alderney Race conditions (a potential tidal site in French water) has been considered.

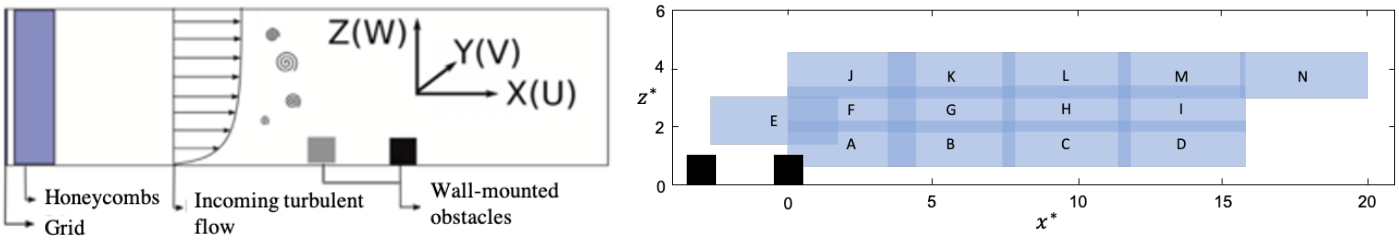

Figure 1. Schematic view of the experimental set-up.

To characterize the flow, Particle Image Velocimetry (PIV) measurements are successively conducted in three spanwise planes: $y0$, $y1$ (at H of $y0$) and $y2$ (at $2H$ of $y0$). In each spanwise plane (represented in yellow figure 2), PIV measurements are performed on 14 PIV planes. Figure 1 (right) presents their spatial organization in the symmetrical median plane $y0$ which is quite similar to the two other spanwise planes. Before PIV measurements, the tank is seeded with 10μm diameter silver coated glass micro-particles. Particles illuminated by a $200mJ$ Nd-Yag laser is detected on 3 to 5 pixels. Cross-correlation is used to calculate particule displacement between two images and outliers are replaced with the Universal Outlier Detection method. PIV acquisitions are made during 150s, hence 2250 double images are taken with a 15Hz acquisition frequency. Plane dimensions are $1153 \times 430\text{mm}^2$ with a spatial resolution of $dx = dz = 11.6$mm. The reader is referred to previous works [7] for details about experimental set-up and the measurement method.

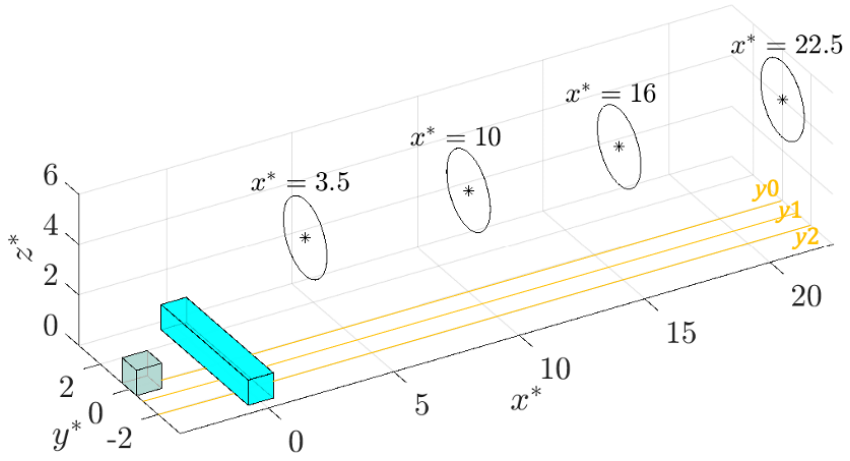

Figure 2. Turbine at its four different positions for $C1$-$C6$ (grey cube + blue cylinder) and $C6$ (blue cylinder) cases. Yellow lines representing the PIV spanwise planes (PIV measurement done without the turbine).

2.2 Turbine presentation

To study the effect of these two bathymetry-like obstacles on tidal turbine, a three-bladed horizontal axis turbine is positioned in the obstacles wake (see figure 3). This turbine has been developed at IFREMER and was first presented in [13]. The turbine blades are rigid and their open geometry is described in [5, 14]. The rotor diameter is $D = 0.724\text{m} \approx 3H$. The turbine rotation speed is controlled with no blade pitch modification. The torque (Q) and the thrust (T) applied on the main rotation axis are measured without any mechanical friction. The sampling frequency of the turbine sensors is 120 Hz. For this study, the turbine is fixed successively at 4 different positions in the flume tank $x = 3.5H$, $10H$, $16H$ and $22.5H$, at mid-depth (hub at $z^* = 4$) (figure 2 and 3). The following notations will be used: $x^* = x/H$, $y^* = y/H$ and $z^* = z/H$.

Experiments are done for different Tip Speed Ratios (TSR): 0, 3, 4 and 5, with TSR the ratio between the blade tip rotational speed and the upstream flow speed: $TSR = \frac{\omega R}{U_\infty}$.

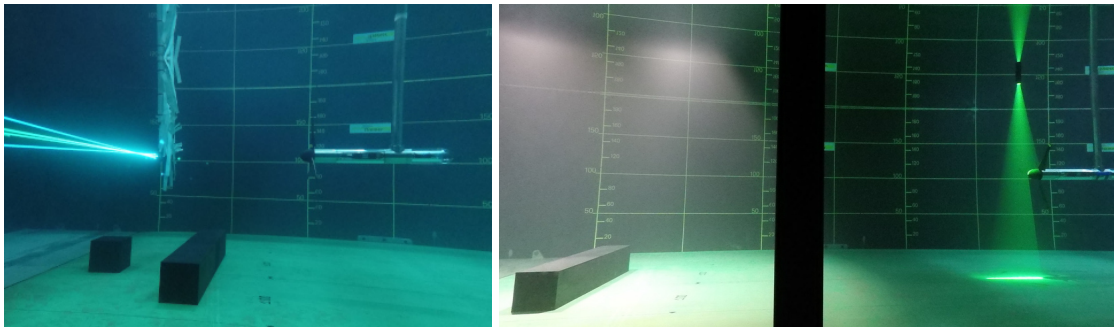

Figure 3. Picture of the experimental turbine during experiments. Case $C1$-$C6$ on the left (turbine located at $x^* = 3.5$) and C6 on the right (turbine located at $x^* = 16$).

3. Input flows characterization

3.1 Mean flow and turbulence statistics

Figures 4, 5 and 6 present respectively the mean streamwise velocity, the mean vertical one and the Reynolds stress $\tau_{uw} = \overline{u'w'}$ donwstream both kind of bathymetry. The classical behaviour of the flow past a wall-mounted element is observed for $C6$. The flow separates at the leading edges of the cylinder into the outer steady region and the recirculation area downstream of the cylinder. A shear layer develops in- between and then the flow reattaches. The wake rise immediately after the obstacle with a 2D behavior between $y-1$ and $y1$ planes [7] and the shear layer has the same upward orientation.
In $y2$-plane, the wakes of both cases are similar looking at mean velocities and shear layer extend but the cube presence upstream the cylinder modifies deeply the flow behavior between $y-1$ and $y1$ planes. We can see on figures 4 and 5 that the wakes are completely different in $y0$ and $y1$-plane, where the cube wake hits the cylinder and mofifies its wake development. In $y0$-plane, the flow separates at the leading edge of the cube. The associated shear layer is forced to accelerate over the cylinder. Behind the cylinder, the recirculation area is small compared to what has been observed for $C6$. The shear layer of the cube develops on top of the cylinder shear layer. After this swerve (from $x^* = 3$), the upper limit of the wake stays at constant height. In $y1$-plane and $y2$-plane, the upper limit of the wake moves slowly toward the surface until $x^* = 20$, where it reaches the same height than in $y0$-plane: $z^*(U = 0.9 * U_\infty) \approx 3.5$.

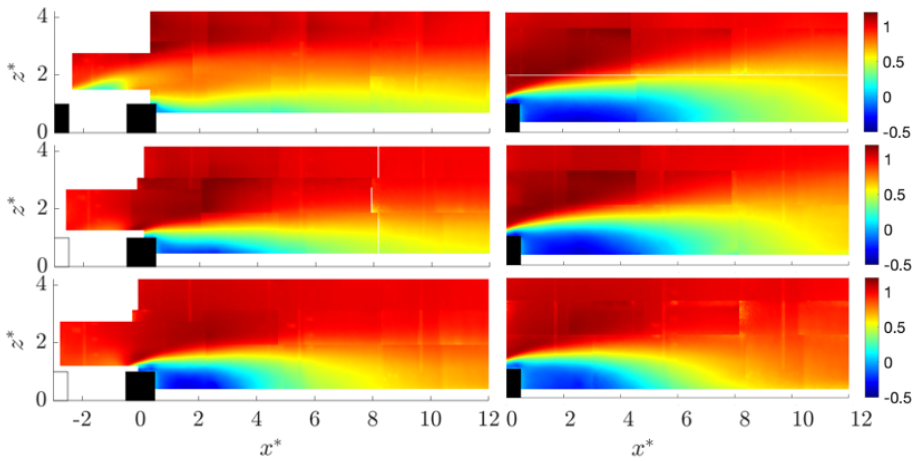

Figure 4. Mean streamwise velocity U, behind $C1$-$C6$ (left) and $C6$ (right). Top: $y0$, middle: $y1$, bottom: $y2$.

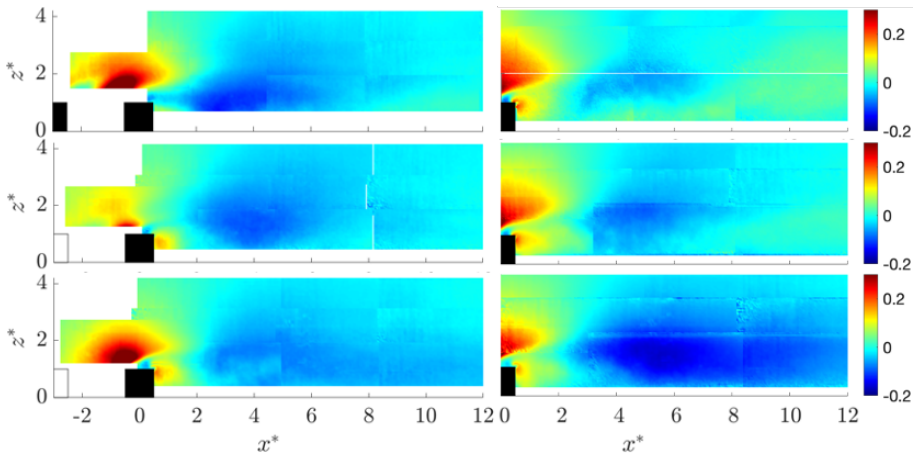

Figure 5. Mean vertical velocity W, behind $C1$-$C6$ (left) and $C6$ (right). Top: $y0$, middle: $y1$, bottom: $y2$.

The average Reynolds shear stress τ_{uw} presented in figure 6 is a good marker of the shear layer developing between the outer undisturbed flow and the recirculation region and of the generated turbulence. Shear layers appear smaller in $C1$-$C6$ wake compared to the $C6$ one. In $y2$-plane, shear layers are really similar. In $y0$ and $y1$-plane, $C6$ shear layer has the same upward orientation, that is not present at all in $C1$-$C6$ wake. For $C1$-$C6$, the overlay of the two shear layers, coming for the cube on top and the cylinder behind, is clearly noticeable. The cube shear layer inhibits the rising of the cylinder shear layer.
So, globally, the cube wake inhibits the development of the energetic and directed upward wake of the cylinder. The assumption made in [7] that the flow can be considered 2D, by symetrey between the planes $y-1$ and $y1$ in the cylinder case can not be done for the $C1$-$C6$ configuration.

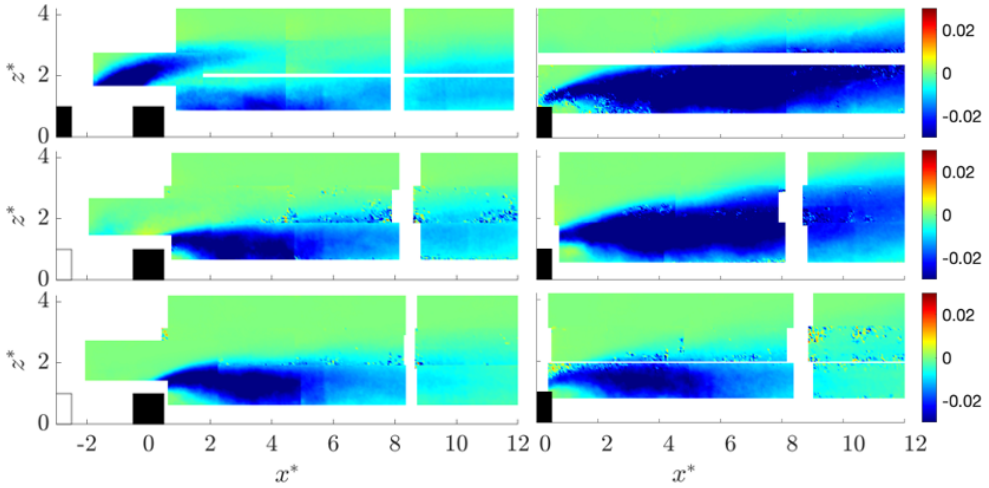

Figure 6. Average Reynolds shear stress τ_{uw} behind $C1$-$C6$ (left) and $C6$ (right). Top: $y0$, middle: $y1$, bottom: $y2$. Note that some areas suffer from the poor lightning and data in these area are not fully converged.

3.2 Characterization of the wake flow organization

3.2.1 Spectral content

To better compare the two kinds of wakes, the focus is done on structures shed by the obstacles. To do so, we choose to plot the Power Spectral Density (PSD) of the fluctuating streamwise velocity along a vertical line, that corresponds to the middle of a block of 3 vertical planes (e.g. A, F and J, for $x^* = 2.2$). For all computations, each velocity signal is splitted over window intervals of 1024 points (using a Hanning window) and with 50% overlap. PSD normalization is the same for all figures presented. Spectra are plot as function of

the Strouhal number: $St = \frac{fH}{U}$. Note that when plotting the PSD, at one point, as function of the frequency, the $-5/3$ slope characteristic of the inertial range of the energetic cascade of turbulence is observed, confirming thus the dissipation process. The choice is made to compare PSD map in the symmetry plane of $C1$-$C6$ (figure 7) to PSD map in the symmetry plane of $C6$ (figure 8), where wakes have the stronger differences.

First, results deduced from an isolated cylinder wake flow confirm that large scale periodic structures develop in the wake with a characteristic Strouhal number of 0.07 [7]. The rising of these flow structures in the far wake is clearly indicated as their footprint are present in the upper measurement planes ($z^* > 3.5$). This Strouhal value is similar to previous cylinder wake investigations [8].

Second, for $C1$-$C6$ configuration, in the $y0$-plane, the near cube wake is dominated by a vortex shedding frequency corresponding to a Strouhal number around 0.1. Furthermore, a frequency peak at $St \approx 0.16$ emerges, characterizing the cube-cylinder wake interaction. This value corresponds to the sum of the cube wake vortex-shedding frequency and the cylinder wake vortex-shedding frequency. Downstream the obstacles, even if various frequency peaks are distinguishable due to the 3D flow interactions, $St \approx 0.07$ peak remains. In the far wake field, some periodic flow structures characterized by $St \approx 0.07$ are present and they are related to the same flow structure frequency passage behind an isolated cylinder [7]. However, this frequency peak is only obtained for $z^* < 3.5$.

By comparison with the isolated cylinder, PSD results emphasize that similar large scale structures develop in the far field, but they don't rise in the water column. They only move horizontally in the far wake.

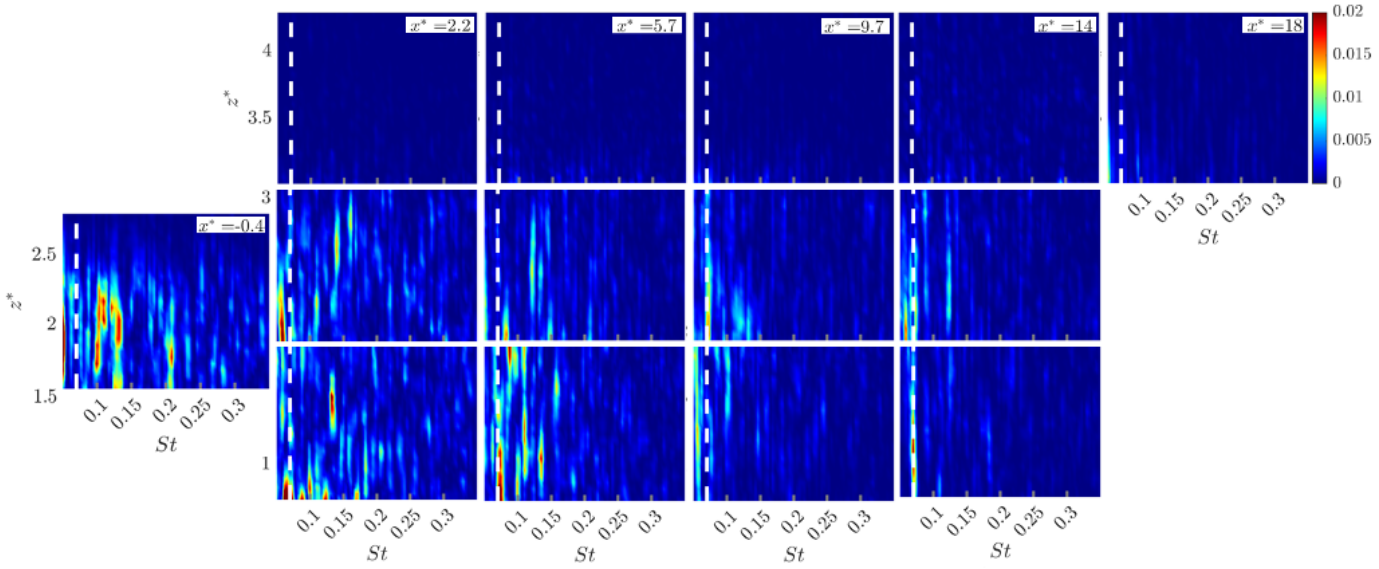

Figure 7. $C1$-$C6$ PSD maps of the fluctuating streamwise velocity component u', at $x^* = -0.4, 2.2, 5.7, 9.7$, 14 and 18. Dashed white line corresponds to $St = 0.07$.

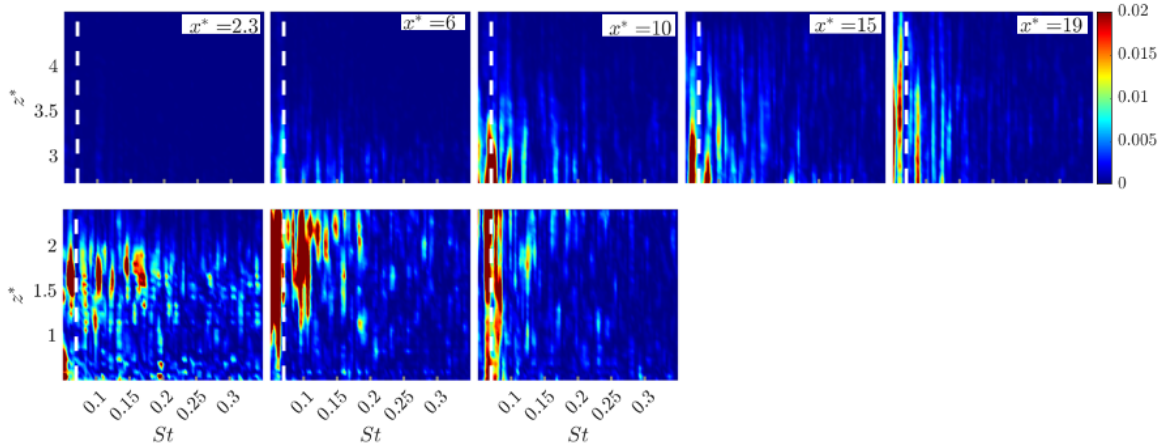

Figure 8. $C6$ PSD maps of the fluctuating streamwise velocity component u', at $x^* = 2.3, 5.8, 10$ 14 and 18. Dashed white line corresponds to $St = 0.07$.

3.2.2 Flow velocity characterization

The focus is now made on the size of the structures that will impact turbines. To retrieve characteristic length scales of vortex structures emitted by the obstacles, spatial autocorrelation $R_{i'i'}$ is used as presented in [15]. $R_{i'i'}$ ($i' = u', w'$) is calculated for both velocity components as follows:

$$R_{u'u'}(x^*_{ref}, z^*_{ref}, x^*, z^*) = \frac{\overline{u'(x^*_{ref}, z^*_{ref})u'(x^*, z^*)}}{\sqrt{\overline{u'^2(x^*_{ref}, z^*_{ref})}}\sqrt{\overline{u'^2(x^*, z^*)}}} \quad (1)$$

where (x^*_{ref} ,z^*_{ref}) are the coordinates of a fixed reference point. As an illustration, figure 9 presents $R_{u'u'}$ and $R_{w'w'}$ map for $(x^*_{ref}, z^*_{ref}) = (2.6, 2.6)$ in $C1$-$C6$ symmetrical $y0$-plane where the 0.6-contour level is plotted (black ellipse). This rather high contour value has been chosen to have statistically good accuracy while focus on large-scale events [16]. Using these isopleths, the streamwise and vertical size of vortex structures can be estimated. This length corresponds to the double grey arrows indicated in figure 9. Even if the threshold level of 0.6 leads to an underestimation of vortex structure length scales by comparison to the classical integral scales, it allows a qualitative analysis of the flow structures. As the inclination of the structures is small, the length estimation is done along x and z-axis. We denote $l^*_{u_x}$ and $l^*_{w_z}$ the size of the isopleth ellipses $R_{u'u'}$ along x and $R_{w'w'}$ along z respectively.

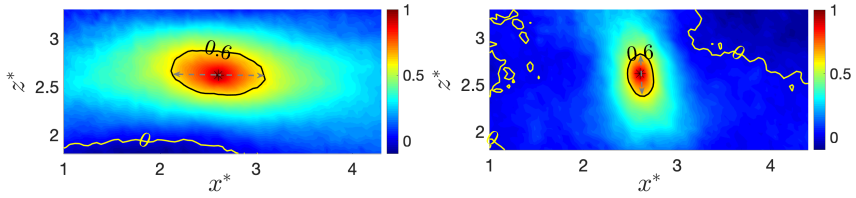

Figure 9. $C1 - C6$ two-point correlation maps $R_{u'u'}$ (left) and $R_{w'w'}$ (right) obtained at a reference point $x^*_{ref} = 2.6$, $z^*_{ref} = 2.6$ in the symmetrical $y0$-plane. Black lines: $R_{i'i'} = 0.6$. Yellow lines: $R_{i'i'} = 0.0$.

Figure 10 and 11 present the evolution of the length scales as a function of z^* for selected x^*-positions. Slight discontinuities appear due to in-between measurements plane. Globally, length scales are larger in $C6$ wake than in $C1$-$C6$ wake. More precisely, they achieved $l^*_{u_x} = 1.2$ in the wake of the composed bathymetry where the maximum length scale of the structure is $l^*_{w_z}$=2 in the cylinder wake. The other main difference is that the cylinder wake extends higher contrary to the tandem configuration wake, where no structure attend higher than $z^* \approx 3.5$. It is expected that these length scales evolve similarly than the classical integral scales.
$C1$-$C6$ wake is divided in two parts. In the upstream one ($x^* = 2.2$ and 5.7), the wake is 3D. Elongated structures ($l^*_{u_x} >> l^*_{w_z}$) can be found in precise location as in the shear layer of the cube ($y0$-plane, $z^* \approx 2.8$) or in the shear layer of the cylinder($z^* \approx 1$ ($y1$-plane) and $z^* \approx 1.3$ ($y2$-plane)). Thus, in the upper region of the wake, the flow is not homogeneous along the transverse axis y. Downstream, the flow becomes more homogeneous, the wake can be treated as 2D.
$C6$ shedding vortices have a totally different development. Along y-axis, structures are only similar upstream in the wake. $3H$ downstream the cylinder, structures passing in $y2$-plane are totally different from the one in $y0$ and $y1$-plane due to the side effect of the cylinder, and become very elongated in the bottom part of the water column from $x^* \approx 14$. In $y0$ and $y1$-plane, structures are less elongated and reach their maximum spatial extension from $x^* \approx 5.7$. They are tall in almost all the water column, with a maximum at around $z^* \approx 3$.
To sum up, these two wakes develop a different way the one from the other. The upstream presence of the cube leads to an annihilation of the wake movement towards the surface in the median plane obstacles. This comes with a strong reduction of the turbulent structures length scale, especially downstream. These difference between both wakes will give different turbine behaviour to the flow.

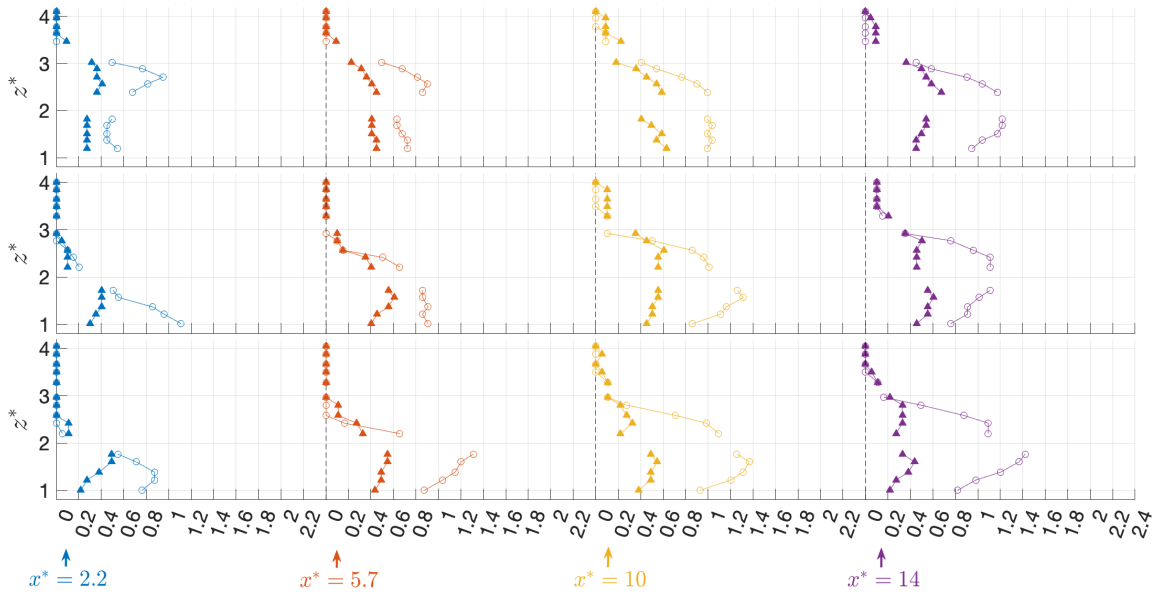

Figure 10. z-profiles of the streamwise ($l^*_{u_x} \iff \circ$) and vertical ($l^*_{w_z} \iff \blacktriangle$) length scales of $C1$-$C6$. Top $\iff$ y0-plane, middle $\iff$ y1-plane, bottom $\iff$ y2-plane.

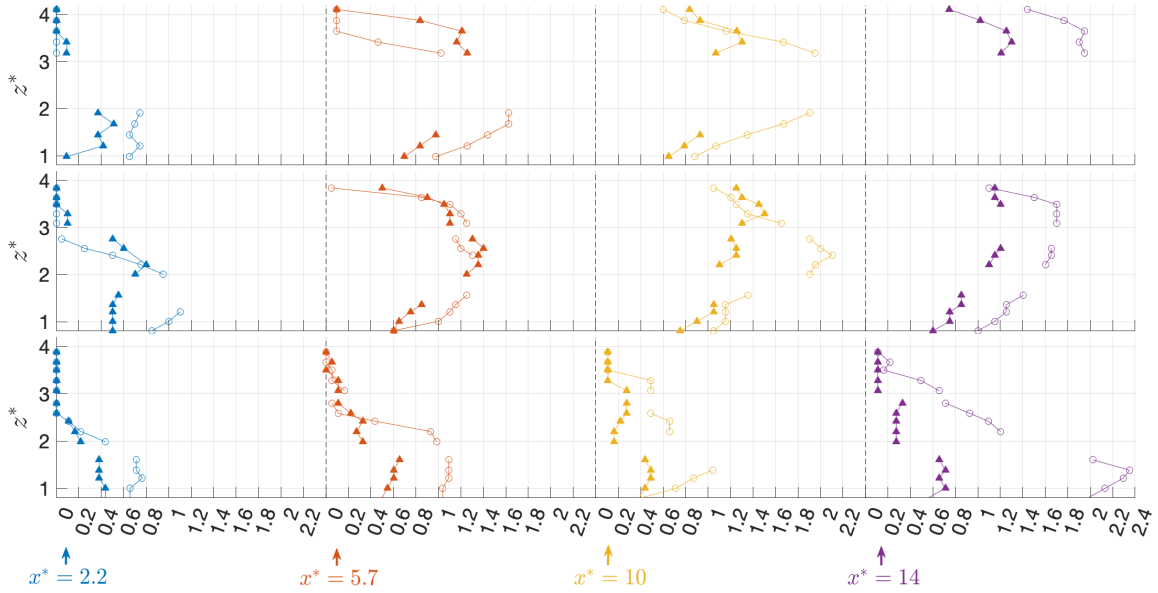

Figure 11. z-profiles of the streamwise ($l^*_{u_x} \iff \circ$) and vertical ($l^*_{w_z} \iff \blacktriangle$) length scales of $C6$. Top $\iff$ y0-plane, middle $\iff$ y1-plane, bottom $\iff$ y2-plane.

4. Wake effects on turbine performances

The wake of $C1$-$C6$ bathymetry develops horizontally in $y0$-plane after $x^* = 3$ and reaches $z^* = 3.5$. In $y1$-plane and $y2$-plane, the upper limit of the wake moves slowly toward the surface until $x^* = 20$, where it reaches the same height than in $y0$-plane: $z^*(U = 0.9 * U_\infty) \approx 3.5$. Thereby, further the turbine from obstacles, further its is immersed in the wake. This is not happening in the symmetry plane $y0$ but around it, where the wake rises with x^*. Behind $C6$ bathymetry, contrary to behind the tandem case, the wake rises immediately after the obstacle in $y0$ and $y1$-plane. Thereby, the farer the turbine from the obstacles, the more immersed in the cylinder wake. Moreover, turbines are submitted to turbulent structures of various sizes depending of where they are in the wake (figures 10 and 11). Behind $C1$-$C6$, the bottom of the part of the swept area receives elongated structures where no structures impact its upper part. More precisely, upstream, these elongated structures are hitting the swept area only on $y0$. They start hitting its side (in $y1$ and more) after $x^* \approx 10$. Behind $C6$, from $x^* \approx 5.7$, the bottom half part of the turbine is submitted to large and rather round structures.

From $x^* \approx 10$, the turbine swept area may received large and a bit elongated structures. These structures are two time higher (along z^*) and almost two time longer (along x^*) than structures observed in $C1$-$C6$ wake.

4.1 Performances comparison

To compare the effects of these two wakes on tidal turbines, the power coefficient C_P is used:

$$C_P = \frac{Q\omega}{\frac{1}{2}\rho S U^3} \tag{2}$$

where Q is the mean hydrodynamic torque (in N·m), and S the swept area. The angular velocity of the turbine is represented by ω in rad/s. In the following C_P is calculated with both the incoming flow velocity, $C_P(U_\infty)$, and the local velocity values, $C_P(U_{x^*})$ (preliminary measured at the centre rotor position), see Table 1.
Figure 12 presents the mean power coefficient as fonction of its TSR, for different streamwise positions for both cases. Error bars present the C_P standard deviations. For both cases, all the C_P curves have the same behaviour that in [13] with a maximum at $TSR = 4$. When looking on $C_P(U_\infty)$, both performance coefficients decrease with the turbine going downstream, as their standard deviations increase. So, here, the farer and the deeper in the wake, the less power and the more variability. Blackmore et al. [4] observed that an increase of the turbulent intensity causes the decrease of the C_P of the turbine at a given TSR, but that increase of integral scales of turbulence causes the increase of C_P (and C_T). The effect of integral scales is described as stronger than the one of the turbulent intensity. At $x^* = 3.5$, C_P standard deviation in the wake of $C6$ is at most 1.3 times larger than in the wake of $C1$-$C6$. At $x^* = 22.5$, C_P standard deviation in the wake of $C6$ is at most 3.3 times larger than in the wake of $C1$-$C6$. $C6$ wake is always responsible of stronger fluctuations than the $C1$-$C6$ one.

Case \ Turbine position	$x^* = 3.5$	$x^* = 10$	$x^* = 16$	$x^* = 22.5$
$C1-C6$	1.08	1.04	1.00	0.99
$C6$	1.05	0.98	0.91	0.91

Table 1. Local velocity values (U_{x^*}) for the fourth positions in the wake of the two cases

The over-estimation of C_P when calculated with the incoming flow velocity can be corrected by taking into account the local flow velocity measured at the location of the rotor before turbine installation (results presented Part. 2). The results presented figure 12 (bottom) show a less marked trend, with a reverse evolution with the turbine spacing with the obstacles. In this case, $C_P(U_{x^*})$ is higher far away in the wake than when the turbine is close to the obstacles. These results show that with this kind of flow presenting a marked vertical velocity profile and 3D effects, a point velocity measurement is not enough to calculate the power coefficient. The knowledge of the velocity characteristics over the rotor swept area is needed.

4.2 Flow-turbine correlation

PSD of the power $P = Q\omega$ is plotted (figure 13) at $x^* = 22.5$ and for $TSR = 4$, behind both bathymetry. Globally, both spectra follow the slope $-11/3$ which is in agreement with previous works ([9] and [17]). Both spectra present a peak at 5.28 Hz that corresponds to 3 times the rotation frequency ($f_r = 1.76$ Hz). This peak is linked to the 3 blades feeling different loads when rotating. This peak is not followed by its first harmonic, like it is for the thrust PSD at 10.5 Hz. Indeed, for $f > 3.f_r$, both spectrum are superimposed, showing a high frequency filter on the energy caption. At low frequency, spectra differ. In fact, when the turbine is immersed in $C6$ wake, the periodic passage shedding structures is clearly visible. This corresponds to the high PSD level visible around $f = 0.018$ Hz, so at Strouhal number of 0.07. In this case, the wake development plays an important role and the frequency signature of the energetic flow events is well found in the turbine response.

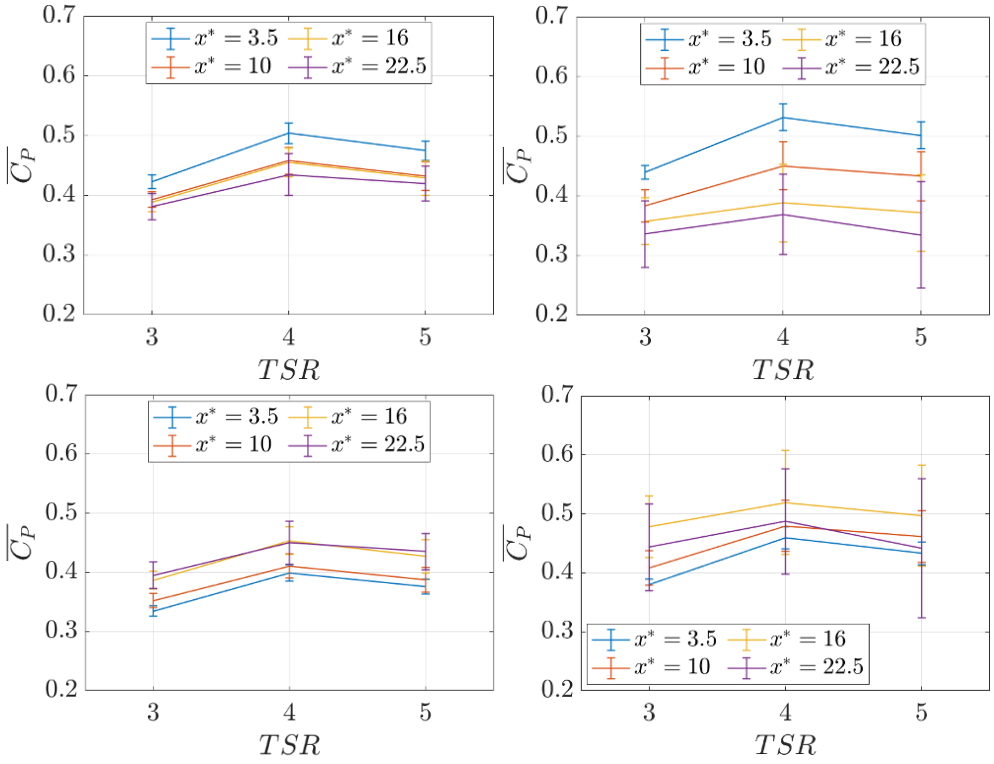

Figure 12. Power coefficient for $C1$-$C6$ (left) and $C6$ (right) cases calculated with U_∞ (top) and with U_{x^*} (bottom).

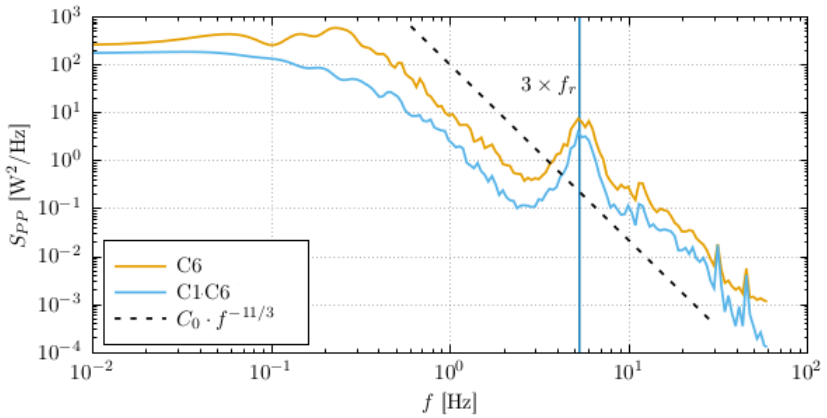

Figure 13. PSD of the power at $x^* = 22.5$ and for $TSR = 4$, for both bathymetry.

To confirm the points above, figure 14 presents the standard deviation of the power coefficient as function of the standard deviation of the streamwise velocity for both cases, plain dots for $C6$ and empty diamond for $C1$-$C6$ (for the three TSR). When the turbine is in the wake of $C1$-$C6$, both fluctuations of C_P and U are small with $\frac{\sigma(C_P)}{\overline{C_P}} < \frac{\sigma(U)}{\overline{U}}$. This confirms the PSD results showing that there is no low frequency events perceived by the turbine and that the rotor filters the high frequency flow variations. For the case $C6$, the flow variations are always higher than for the previous case, with a higher impact on the power coefficient. These results highlight how the rotor can positively answer to that kind of sollicitations. In this case, the low frequecy energy content is well recover by the turbine, confirming the tendancy previously anticipated.

5. Conclusion

The wake past obstacles representative of seabed elements is investigated. Two case studies are compared. First, the classical case of an isolated wall-mounted cylinder is studied. Its wake is energetic and develops towards the surface in its symmetry plane. Vortices shed due to the interaction cylinder-flow are reaching

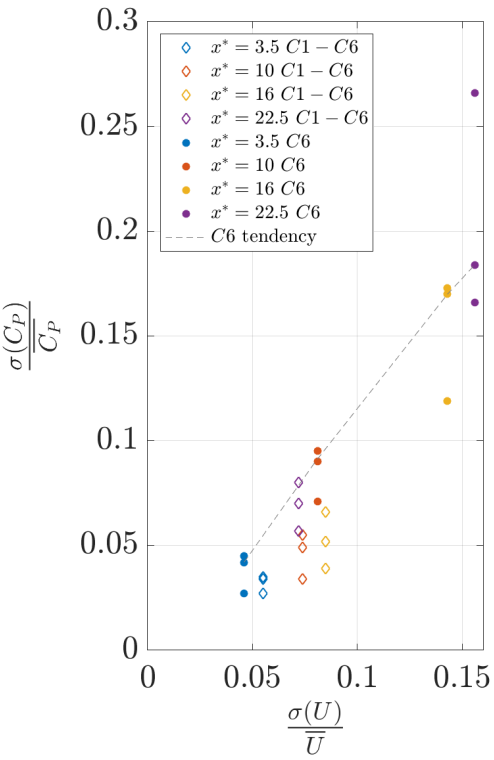

Figure 14. C_P variations as function of streamwise velocity variations for the two cases.

the surface, creating kolk. These vortices are large in the median part of the cylinder. When a cube is added upstream the cylinder, its presence has a strong impact on the cylinder wake development (not behind the cylinder extremities until $y2$). The wake of the tandem case is less energetic and develops horizontally. Structures shed by the $C1$-$C6$ configuration are almost two times smaller that the one coming from the isolated cylinder. Hence, the presence of an obstacle upstream of a large aspect ratio element is not negligible on the wake development. When looking on the impact of both wakes on tidal turbines, it is hard to conclude properly. C_P is adimensioned by the inlet velocity so the impact of the local velocity, the induction zone and 3D effects are overlooked. C_P fluctuations increase with the size of vortices increasing. Moreover, mean hydrodynamic thrust is sensible to the vortex shedding frequency of the isolated cylinder but not of the tandem.
These results give complementary informations on the interaction between a turbulent flow and a tidal turbine (complementary to studies based on grid turbulence). Indeed, the isolated cylinder is really demanding for the tidal turbine, although the tandem case is possibly more representative of what can be encountered in operation.

Aknowledgement

This work benefits from a French state grant managed by the National Research Agency, France under the Investments for the Future program bearing the reference ANR-10-IEED- 0006-11 (ANR-FEM THYMOTE). This project was partly financially supported by the European Union (FEDER), the French government, IFREMER and the region Hauts-de-France in the framework of the project CPER 2015–2020 MARCO ; the European Union's Horizon 2020 research and innovation programme for RealTide project under grant agreement No 727689 and the support of the Met-Certified project, funding from the Interreg 2 Seas programme 2014-2020, co-funded by the European Regional Development Fund under subsidy contract N. 2S01-020. The authors would like to gratefully acknowledge Maria Ikhennicheu, Thomas Bacchetti and Jean-Valery Facq involved in the experimental database generation.

References

[1] K. McCaffrey, B. Fox-Kemper, P. E. Hamlington, and J. Thomson, "Characterization of turbulence anisotropy, coherence, and intermittency at a prospective tidal energy site: Observational data analysis," *Renewable Energy*, vol. 76, pp. 441–453, 2015.

[2] P. Mercier, M. Grondeau, S. Guillou, J. Thiébot, and E. Poizot, "Numerical study of the turbulent eddies generated by the seabed roughness at a tidal power site," *Applied Ocean Research*, vol. 97, 2020.

[3] L. Chamorro, C. Hill, S. Morton, C. Ellis, R. Arndt, and F. Sotiropoulos, "Interaction between a turbulent open channel flow and an axial-flow turbine," *Journal of Fluid Mechanics*, vol. 716, p. 658–670, 2013.

[4] T. Blackmore, L. Myers, and A. Bahaj, "Effects of turbulence on tidal turbines: Implications to performance, blade loads and condition monitoring," *Int. Journal of Marine Energy*, vol. 14, pp. 1–26, 2016.

[5] P. Mycek, B. Gaurier, G. Germain, G. Pinon, and E. Rivoalen, "Experimental study of the turbulence intensity effects on marine current turbines behaviour.," *Renewable Energy*, vol. 66, pp. 729–746, 2014.

[6] M. J. Churchfield, S. Lee, J. Michalakes, and P. J. Moriarty, "A numerical study of the effects of atmospheric and wake turbulence on wind turbine dynamics," *Journal of Turbulence*, vol. 13, p. N14, 2012.

[7] M. Ikhennicheu, G. Germain, P. Druault, and B. Gaurier, "Experimental study of coherent flow structures past a wall-mounted square cylinder," *Ocean Engineering*, vol. 182, pp. 137–146, 2019.

[8] M. Omidyeganeh and U. Piomelli, "Large-eddy simulation of two-dimensional dunes in a steady, unidirectional flow.," *Journal of Turbulence*, vol. 42, pp. 1–31, 2011.

[9] B. Gaurier, M. Ikhennicheu, G. Germain, and P. Druault, "Experimental study of bathymetry generated turbulence on tidal turbine behaviour," *Renewable Energy*, vol. 156, pp. 1158–1170, 2020.

[10] M. Ikhennicheu, G. Germain, P. Druault, and B. Gaurier, "Experimental investigation of the turbulent wake past real seabed elements for velocity variations characterization in the water column," *International Journal of Heat and Fluid Flow*, vol. 78, 2019.

[11] R. Martinuzzi and J. Havel, "Vortex shedding from two surface-mounted cubes in tandem," *Int. J. Heat Fluid Flow*, vol. 25, no. 3, pp. 364–372, 2004.

[12] T. Kim and K. Christensen, "Flow interactions between streamwise-aligned tandem cylinders in turbulent channel flow," *AIAA J.*, vol. 56, no. 4, pp. 1–13, 2018.

[13] B. Gaurier, S. Ordonez, J. Facq, G. Germain, F. Salvatore, I. Santic, T. Davey, C. Old, and B. Sellar, "MaRINET2 tidal energy RR tests - Performance comparison of a hat subjected to combined W. and C. conditions," *Journal of Marine Science and Engineering*, vol. 8, p. 463, 2020.

[14] B. Gaurier, G. Germain, J. Facq, A. Grant, A. Day, E. Nixon, F. Di Felice, and M. Costanzo, "Tidal energy RR tests comparisons between towing and circulating tanks results," *Int. Journal of Marine Energy*, vol. 12, pp. 87 – 109, 2015.

[15] M. Magnier, P. Druault, and G. Germain, "Wall-mounted cylinder wake rising annihilation in presence of an upstream cube," *Under review in European Journal of Mechanics - B/Fluids*, 2020.

[16] P.-A. Krogstad and R. A. Antonia, "Structure of turbulent boundary layers on smooth and rough walls," *Journal of Fluid Mechanics*, vol. 277, p. 1–21, 1994.

[17] H. Liu, Y. Jin, N. Tobin, and L. Chamorro, "Towards uncovering the structure of power fluctuations of wind farms," *Physical Review*, vol. 96, 2017.